Pattern Recognition on the Structure−Activity Relationship of Nano Pt−Ru Catalysts: Methodology and Preliminary Demonstration

Qingye Lu, Bo Yang, Lin Zhuang,* and Juntao Lu

Department of Chemistry, Wuhan University, Wuhan 430072, China

Received: February 8, 2005; In Final Form: March 8, 2005

The activity of nano Pt−Ru catalysts is a multivariate function of particle size, alloyed degree, oxide composition, and so forth. The monodependencies of catalytic activity on individual structure parameters (structure−activity relationship, SAR) are of great importance but, unfortunately, unobtainable in practical measurements. A pattern-recognition methodology is proposed for the first time to extract SAR information from all of the relative experimental data, which we hope will cast new light on the in-depth understanding of this important catalyst. As a preliminary demonstration, a multivariate linear regression and a generalized regression neural network were applied to analyze a small data set for methanol oxidation. It was found that both increasing the content of hydrous ruthenium oxides and decreasing the particle size would benefit the catalytic activity, whereas the effect of the Pt−Ru alloy degree turned out to be unremarkable.

1. Introduction

The Pt−Ru binary catalyst is currently the most important anode catalyst for direct methanol fuel cells (DMFC) and proton exchange membrane fuel cells (PEMFC) fed with reformed gas.[1−6] Although quite a few researchers were devoted to developing ternary, or even quaternary, catalysts (Pt−Ru−X, X = W, Os, Sn, etc.),[7−12] the thus-improved activity was slight, while difficulty and cost have much increased in catalyst preparation; there have hitherto been no commercial Pt−Ru−X catalysts.

The promotion effect of Ru in the Pt−Ru catalyst has been well documented to follow a bifunctional mechanism.[13−19] In brief, the presence of Ru accelerates the water-discharge step

$$Ru + H_2O \rightarrow Ru{-}OH_{ads} + H^+ + e^- \qquad (R1)$$

the product of which, OH_{ads}, is the key species for removing poison intermediates blocking the Pt surface ($Pt{-}CO_{ads}$)

$$Pt{-}CO_{ads} + Ru{-}OH_{ads} \rightarrow Pt + Ru + CO_2 + H^+ + e^- \qquad (R2)$$

which is the rate-determining step in the overall reaction. Although some active metals, such as Sn, Mo, Fe, and so forth, were thought to be able, or even better, to play the role of Ru in reaction 1, Ru has been proven in past decades to be the best secondary element in Pt-based binary catalysts.[1−6] After systematic investigations, Johnson-Matthey, the leading catalyst company, even declared abandoning exploration of Pt-based catalysts other than Pt−Ru, and concentrating on the optimization of the Pt−Ru catalyst.[3]

1.1. Necessity and Difficulty of Structure−Activity Relationship Study for Nano Pt−Ru Catalysts. Although Pt−Ru has been investigated since the 1960s,[20] the structure−activity relationship (SAR) of the Pt−Ru catalyst, especially the nano Pt−Ru particle dispersed on high-specific-surface carbon supports (Pt−Ru/C), has not been fully understood. The reason for this is mostly due to the variability of Ru, which could exist as an Ru metal, a Pt−Ru alloy, and Ru oxides (RuO_x), including hydrous oxides (RuO_xH_y). Furthermore, the structure of Ru oxides is various and difficult to characterize. For example, our recent study revealed that there were at least two kinds of Ru oxides in Pt−Ru/C, which played opposite roles in catalysis.[21] These complex factors greatly hinder the controllable preparation of nano Pt−Ru catalysts with well-defined structures and the SAR study.

According to the bifunctional mechanism, Ru sites are required to locate close enough to the Pt sites to guarantee reaction 2. In early studies, the Pt−Ru alloy was emphasized because the possible electronic effect between Pt and Ru atoms was also thought to be important, which could reduce the bonding strength between Pt and CO_{ads}, and thus benefit the catalysis.

It remains an open question whether the bifunctional effect or the electronic effect is predominant. In recent years, Rolison et al.[22−25] strongly advocated avoiding the Pt−Ru alloy; they found that the catalytic activity would increase by orders of magnitude if Ru existed in the hydrous oxide form in comparison with that in the alloyed form. The benefits of RuO_xH_y were attributed to the conductibility of its electrons and protons and the innate possession of the surface OH group. A study from Los Alamos National Laboratory (LANL)[26] also showed that the higher the RuO_xH_y content in the nano Pt−Ru catalyst, the better the DMFC performance; in addition, Nafion was much less required in the anode because of the protonic conductivity of RuO_xH_y. However, they also pointed out that RuO_xH_y was not the prerequisite; high DMFC performance was also achieved in their work using a completely alloyed Pt−Ru catalyst.

Despite the fact that the preferable Ru form is still under debate, two conclusions can be drawn from the existing studies: First, the Pt−Ru alloyed degree and the content of

* Corresponding author. E-mail: lzhuang@whu.edu.cn. Fax: +86-27-68754067.

10.1021/jp050700w CCC: $30.25
Published on Web 04/06/2005

hydrous Ru oxides are two important factors determining the catalytic activity of the nano Pt−Ru catalyst. Second, the structures of the current Pt−Ru catalysts are far from optimization, and there is appreciable room for further improvement in catalytic activity. Our recent studies showed that even the should-be-well-optimized commercial Pt−Ru/C catalyst can increase 40% in activity by a simple anodic treatment.[21] Therefore, SAR study of nano Pt−Ru catalysts is highly demanded.

Another important factor determining the mass-specific activity (A_m) is the particle size (ϕ). In principle, if the surface-specific activity (A_s) is unchanged with ϕ, then the smaller the ϕ the higher the A_m. However, A_s is sensitive to the electronic and surface structures of a nano particle, both of which would change with ϕ (quantum size effect). If A_s decreased with ϕ, then a maximum of A_m could be expected at certain ϕ. Another important task of the SAR study is to find the ϕ showing maximal A_m.

For a simple system such as nano Pt/C, the particle size effect for important electrocatalytic processes, for example, oxygen reduction and methanol oxidation, has been well reported.[5,27−34] However, great difficulties have been encountered in the size-effect study for nano Pt−Ru catalysts. Because of the structure variability of nano Pt−Ru, it is very difficult to singly change the particle size while keeping the other sensitive structural factors unchanged, for example, the alloyed degree and the RuO_xH_y contents. Although Takasu et al.[35] and Ren et al.[36] tried to show that the best ϕ for nano Pt−Ru toward methanol oxidation would appear at ca. 3 nm, those results were obtained in neglect of the changes in other structural factors, hence they are of less reliability. Actually, according to our previous studies and the results of this paper, no A_m peak can be observed within a range of ϕ above 2 nm.

1.2. Methodology of Pattern-Recognition Study on SAR of Nano Pt−Ru Catalysts. It is clear, from the above analysis, that the catalytic activity of nano Pt−Ru catalysts is a multivariate function, with key variables including the Pt−Ru alloyed degree (frequently expressed as the Ru fraction in the alloy, x_{Ru}), the particle size (ϕ), and the contents of hydrous Ru oxides (denoted as $m_{RuO_xH_y}$ in this paper). In SAR studies, it is desirable to obtain the monodependencies of A_m on individual factors, for example, $A_m(\phi)$, $A_m(x_{Ru})$, and $A_m(m_{RuO_xH_y})$. Unfortunately, this kind of single-variate SAR is unmeasurable because of the practical difficulty in modulating a single variable exclusively.

In contrast to those previous studies that only looked at one variable with neglect of the influence of other variables, we propose herein a pattern-recognition approach to the SAR study, that is, taking into account all major activity-determining variables and mining the SAR information hiding in the multidimensional data space. The procedure of this approach involves several steps: (1) collecting sufficient typical samples and building up two matrices, one containing the experimental catalytic activity (activity matrix, **A**) and the other consisting of all of the key structural variables (structure matrix, **S**), (2) constructing a mathematical model (**M**) to bridge these two matrices, **M**(**S**)→**A**, and (3) extracting the expected low-dimensional SAR information via model simulation, that is, feeding **M** with a simulating **S** in which only certain structural variable(s) is(are) allowed to change while other variables are kept at specific values. For example, if variable s_1 changes from $s_{1,1}$ to $s_{1,N}$ while other variables, s_2, s_3, ..., and s_M, fix at $s_{2,i}$, $s_{3,j}$, ..., and $s_{M,k}$, respectively

$$\begin{pmatrix} s_{1,1} & s_{2,i} & s_{3,j} & \dots & s_{M,k} \\ s_{1,2} & s_{2,i} & s_{3,j} & \dots & s_{M,k} \\ s_{1,3} & s_{2,i} & s_{3,j} & \dots & s_{M,k} \\ \vdots & \vdots & \vdots & & \vdots \\ s_{1,N} & s_{2,i} & s_{3,j} & \dots & s_{M,k} \end{pmatrix} \xrightarrow{\mathbf{M}} \mathbf{A}(s_1; s_2, s_3, \dots, s_M)$$

then the model prediction **A** (s_1; s_2, s_3, ..., s_M) describes an *explicit* dependence on structural variable s_1 with *parametrical* dependence on the other $M - 1$ variables.

The database construction is the most time-consuming step. After sample collection, the activity matrix (**A**) can be determined from electrochemical measurements, and the structure matrix (**S**) can be obtained from various structure characterizations. For instance, ϕ can be measured from high-resolution transmission electron microscopy (HRTEM) or X-ray diffraction (XRD); x_{Ru} can be estimated from X-ray techniques such as X-ray fluorescence (XRF),[37] XRD,[38,39] or extended X-ray absorption fine structure (EXAFS)[40]; and $m_{RuO_xH_y}$ can be deduced from the results of thermogravimetric analysis (TGA),[24,25,41−43] X-ray photoelectron spectroscopy (XPS),[25,42,44] Synchrotron X-ray Scattering (SXS),[45] X-ray absorption near-edge structure (XANES) and EXAFS,[41] or nuclear magnetic resonance (NMR).[46]

Although the pattern-recognition methodology has been applied widely to solve many chemistry issues involving multivariate, the necessity and the importance of applying such a strategy for the SAR study of nano Pt−Ru catalysts have not been recognized adequately. Obviously, the SAR information obtained from the pattern-recognition study is essentially different from that obtained from unilateral observations. This kind of study will hopefully cast a new light on the in-depth understanding of nano Pt−Ru catalysts.

In the rest of this paper, this methodology is demonstrated quantitatively for the first time with a preliminary data set. Multivariate linear regression (MLR) and the generalized regression neural network (GRNN) are used to model A_m for methanol oxidation over three key structural factors, ϕ, x_{Ru}, and $m_{RuO_xH_y}$. Although the data set currently used in this work is too small to give highly reliable conclusions, the SAR information extracted from the preliminary result is still informative.

2. Experimental Section

The catalysts studied in this work are nano Pt−Ru (20:10 wt %) supported on Vulcan XC72 (Carbot). One of them was from Johnson-Matthey; the others were prepared in our laboratory using the improved impregnation method reported in our previous paper.[42] Catalysts thus-prepared under optimal conditions showed excellent performance for methanol oxidation in comparison with the commercial product and those state-of-the-art catalysts reported in the literature.[21,42] In this work, preparation conditions were altered intentionally to produce catalysts with different structural characteristics (ϕ, x_{Ru}, and $m_{RuO_xH_y}$) and catalytic activities (Table 1), which formed a good collection for pattern-recognition studies on SAR. The values of ϕ and x_{Ru} were calculated from XRD measurements, and $m_{RuO_xH_y}$ is estimated from TGA. The catalytic activity was evaluated by the current of methanol oxidation.

2.1. XRD for ϕ and x_{Ru}. XRD patterns for the catalyst were obtained on a Shimadzu XRD-6000 X-ray diffractometer using a Cu Kα radiation source operating at 40 kV and 30 mA. The characteristic reflections of a Pt face-centered cubic (fcc) structure were shown clearly by XRD, whereas no visible peaks related to tetragonal RuO_2 or hexagonal close-packed (hcp) Ru phases were found (Figure 1).

TABLE 1: Demonstration Database for Pattern-Recognition Study[a]

	samples	structure matrix			activity matrix	
		$m_{RuO_xH_y}$ (%)	$^1/_\phi$ (1/nm)	x_{Ru} (%)	A_m at 0.4V	A_m at 0.5V
no. 1	Pt−Ru(20:10 wt %)/XC72, ethanol as the precursor solvent, 150 °C for 2h in flowing H_2	2.56	0.25	10	32	185
no. 2	as sample #1, followed by 500 °C for 2h in flowing H_2	2.18	0.23	45	9	63
no. 3	as sample #1, followed by 500 °C for 2h in flowing Ar	0.90	0.28	30	5	41
no. 4	as sample #1, followed by 150 °C for 2h in flowing air humidified with 60 °C water	0.51	0.26	47	9	65
no. 5	Pt−Ru(20:10 wt %)/XC72, water as the precursor solvent, 120 °C for 2h in flowing H_2	3.89	0.36	27	51	295
no. 6	Pt−Ru(20:10 wt %)/XC72, Johnson−Matthey product	3.55	0.48	38	61	329
no. 7	Pt−Ru(20:10 wt %)/XC72, ethanol as the precursor solvent, 120 °C for 2h in flowing H_2	2.36	0.37	3	22	133
	mean:	2.28	0.32	28.6		

[a] The structure matrix consists of the RuO_xH_y quantity ($m_{RuO_xH_y}$), the reciprocal of the particle size ($^1/_\phi$), and the Pt−Ru alloyed degree (x_{Ru}); the activity matrix is composed of mass specific activity (mA per mg Pt) at 0.4 and 0.5 V, denoted as A_m at 0.4V and A_m at 0.5V, respectively.

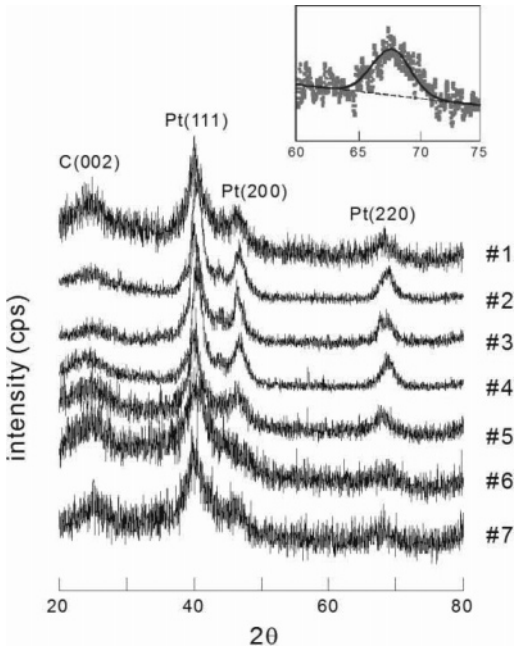

Figure 1. XRD patterns of the samples.

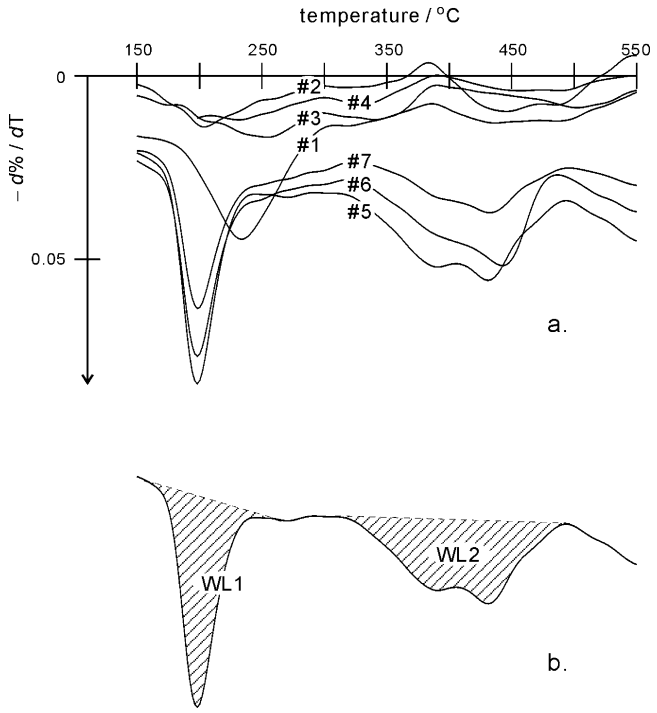

Figure 2. (a) DTG curves of the samples; (b) sketch of the integration of two concerned DTG peaks.

The Pt(220) peak was fitted to a Gaussian line shape on a linear background using the Levenberg−Marquardt algorithm so that the position of the peak maximum (θ_{max}) and the full-width at half-maximum ($B_{2\theta}$) can be obtained precisely.

The lattice parameter of the Pt fcc crystal, a, was calculated from θ_{max} according to Vegard's law

$$a = \frac{\sqrt{2}\lambda_{K\alpha 1}}{\sin \theta_{max}} \quad \text{(E1)}$$

where $\lambda_{K\alpha 1} = 0.154056$ nm.

The diameter of the PtRu nano particles, ϕ, was calculated according to the Scherrer formula:

$$\phi = \frac{0.9\lambda_{K\alpha 1}}{B_{2\theta} \cos \theta_{max}} \quad \text{(E2)}$$

The thus-calculated sizes were in good agreement with those obtained by HRTEM in our experiments.[42]

The Ru atomic fraction in the alloy, x_{Ru}, was calculated from XRD data using the formula proposed by Antolini et al.[38−39]

$$a = a_0 - 0.124x_{Ru} \quad \text{(E3)}$$

where a_0 is the lattice constant of pure Pt. In the case of unsupported pure Pt, $a_0 = 0.39231$, whereas for supported pure Pt, $a_0 = 0.39155$, which was obtained from the XRD measurement of the Pt/C made by E-TEK.[39]

Equation 3 is similar to the formula reported by Radmilović et al.[47] for single-phase Pt−Ru bulk alloys: $a = 3.9262 - 0.1249\ x_{Ru}$ (or $a = 3.8013 + 0.1249\ x_{Pt}$). The validity of eq 3 was verified by the reasonable agreement between the x_{Ru} values deduced using this equation and the values from XRF for the arc-melting Pt−Ru alloys reported by Gasteiger et al.[37]

2.2. TGA for $m_{RuO_xH_y}$. TGA and differential thermal analysis (DTA) were carried out simultaneously on a NETZSCH STA 449C. Samples were tested over the temperature range from room temperature to 800 °C at 10 °C/min under flowing ultrapure N_2. Weight loss was observed in the range of 150−550 °C and was attributed to the structure water of hydrous ruthenium oxides, RuO_xH_y.[24,25,41−43] TGA curves were converted to their differential form (DTG) so that the weight loss step could be better resolved in a peak shape (Figure 2). The area of DTG peaks (WL1 + WL2) within 150−550 °C should be

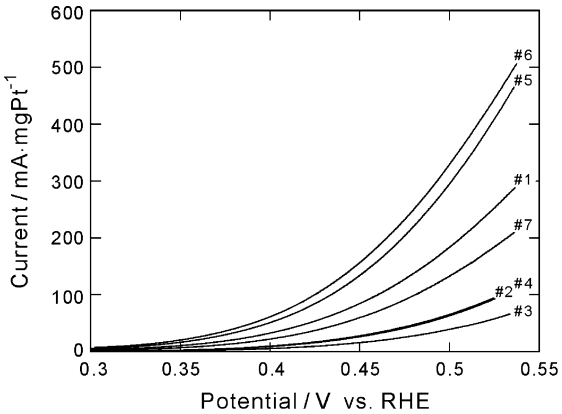

Figure 3. Linear voltammetries (1 mV/s) of the samples in deaerated 0.5 M H_2SO_4 + 1 M MeOH solution at 60 °C.

proportional to the contents of hydrous ruthenium oxides in the catalyst. In this work, we took $m_{RuO_xH_y}$ = WL1 + WL2 for simplicity.

2.3. Electrochemical Evaluation. Pt−Ru/C (10 mg) was dispersed ultrasonically in 1 mL of a diluted Nafion alcohol solution (0.05 wt %), and 5 μL of the suspension was pipetted onto a glassy carbon (GC) substrate (ϕ = 5 mm), which had been buff-polished with an alumina suspension (ϕ = 0.05 μm) prior to use to prepare the working electrode. The coated electrode was dried under an infrared lamp. With careful control of the key experimental details, the error of this operation was controlled within ±5%.

All of the electrochemical experiments were conducted on a CHI-600A electrochemical system. A thermostatic electrochemical cell equipped with the working electrode, a platinum coil counter electrode, and a salt bridge connected to the reference electrode compartment was used for all of the electrochemical measurements. The reference electrode was a reversible hydrogen electrode (RHE)[48] in the same electrolyte as the electrochemical cell. All of the potentials throughout this paper are referred to RHE. All of the solutions were prepared with deionized water (18 MΩ·cm).

A slow linear potential scan (1 mV/s) was carried out at 60 °C in a deaerated 1 M CH_3OH + 0.5 M H_2SO_4 solution to evaluate the catalytic activity for methanol oxidation (Figure 3). Anodic currents at 0.4 and 0.5 V were extracted from the $I-V$ curves and normalized to mass-specific current densities (mA per mg Pt), denoted as A_m at 0.4 V and A_m at 0.5 V, respectively.

3. Results and Discussion

3.1. Mathematical Modeling. Table 1 enumerates the structure matrix (**S**) and the activity matrix (**A**) obtained from XRD and TGA characterizations and electrochemical evaluation, respectively. The reciprocal of the particle size, $^1/_\phi$, representing the catalyst dispersibility, was employed instead of ϕ in constructing **S** for the sake of giving positive correlation to **A**. Two kinds of mathematical methods were applied to model **A** over **S**.

Multivariate linear regression (MLR) is the simplest model that gives only an approximate linear relationship between **A** and **S**:

$$\mathbf{A} = \mathbf{SM} \tag{E4}$$

The linear model (**M**) can be calculated readily by

$$\mathbf{M} = \mathbf{S}^{-1}\mathbf{A} \tag{E5}$$

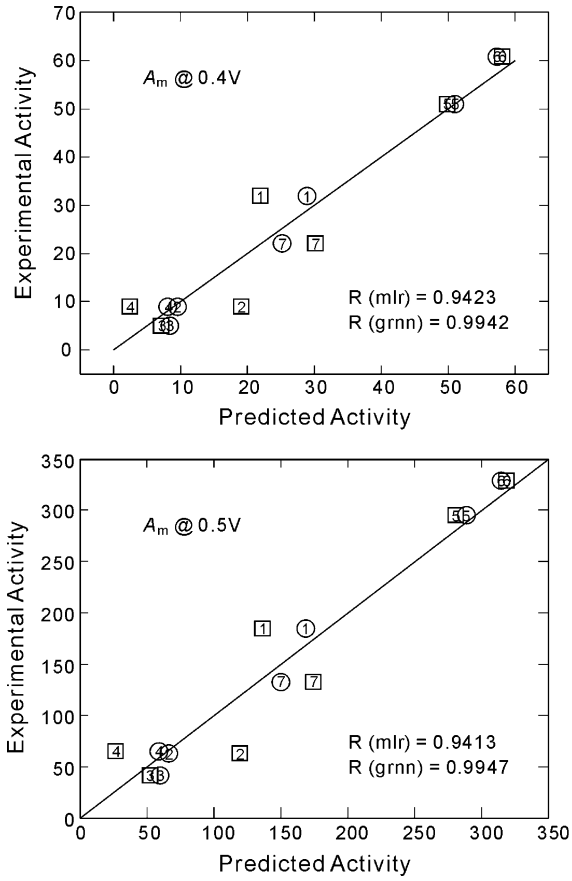

Figure 4. Correlation verifications between the model-predicted activity and the experimental activity at 0.4 and 0.5 V, respectively. Circle points correspond to GRNN modeling; rectangle points correspond to MLR modeling.

where $\mathbf{S}^{-1}$ is the reverse matrix of **S**. Given a simulating structure matrix ($\mathbf{S}_x$), the predicted activity ($\mathbf{A}_x$) can be easily obtained by

$$\mathbf{A}_x = \mathbf{S}_x\mathbf{M} \tag{E6}$$

Despite the simplicity, MLR can provide a qualitative trend of **A** variation with individual structural factors.

In the case of complicated correlations, nonlinear functions are often required to give detailed descriptions. For this purpose, artificial neural networks (ANN) are frequently applied. Feed-forward back-propagation networks (FFBN) are the most popular algorithms in this regard, but, in this work, a generalized regression neural network (GRNN) was found to be more adequate for the current data set. A blank GRNN, **M**, was created and trained with **S** and **A** as input and output, respectively and then the simulating $\mathbf{S}_x$ was input into **M** to get $\mathbf{A}_x$ in order to perform this task.

All of the mathematical processes were realized with MATLAB programs developed by the authors. (The core codes are given in the Appendixes.)

The accuracy of the two models was verified by the correlation between the model-predicted activity and the experimental activity. As shown in Figure 4, all of the points for A_m at 0.4 V and A_m at 0.5 V are located near the straight line $A_{exp} = A_{pred}$, giving correlation coefficients R = 0.94 (MLR) and R = 0.99 (GRNN). It is not surprising that GRNN gives better accuracy because a nonlinear response is always better in a function approximation. It should be pointed out that this kind of correlation verification is a necessary condition only in

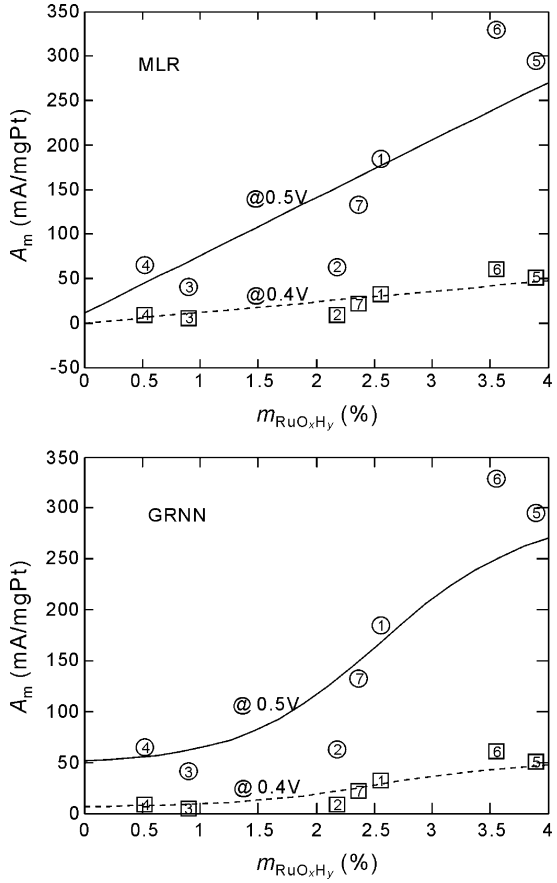

Figure 5. Model prediction A ($m_{RuO_xH_y}$; ϕ, x_{Ru}), describing the explicit dependence of catalytic activity on the contents of RuO_xH_y with parametrical dependence on ϕ and x_{Ru}, which took their mean values in this calculation. The discrete points in the figure are the experimental data, and the continuous lines are the model outputs.

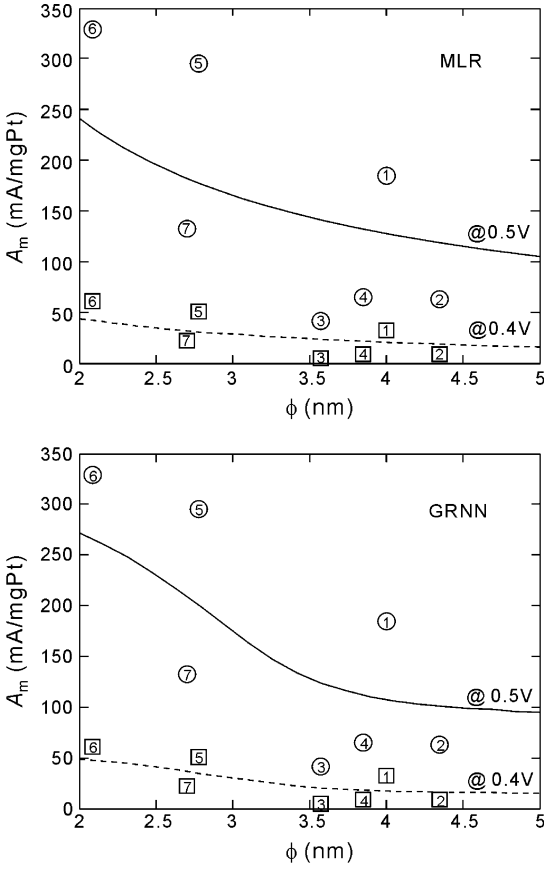

Figure 6. Model prediction A (ϕ; $m_{RuO_xH_y}$, x_{Ru}), describing the explicit dependence of catalytic activity on the particle size with parametrical dependence on $m_{RuO_xH_y}$ and x_{Ru}, which took their mean values in this calculation. The discrete points are the experimental data, and the continuous lines are the model outputs.

evaluating a mathematical model. In principle, a model with a smaller R would cause a larger prediction error, but a model with an extremely high R would not guarantee an appropriate description of the true relationship; over-fitting should be prevented in ANN modeling.

3.2. Model Predictions. Once the mathematical models have been constructed, the monodependencies of A_m on individual structure parameters can be obtained readily. Figures 5−7 show the model predictions A ($m_{RuO_xH_y}$; ϕ, x_{Ru}), A (ϕ; $m_{RuO_xH_y}$, x_{Ru}), and A (x_{Ru}; ϕ, $m_{RuO_xH_y}$) in which all of the model parameters kept the corresponding mean value of the data set (Table 1) and the model variable changed within the original data range. Generally speaking, the model predictions output from MLR and GRNN are in qualitative consistence.

One point should be emphasized before discussing the single-variate SAR pictures individually: the results discussed in this section and in the next section are all based on an imperfect database. The points to be highlighted, therefore, are the way of realizing pattern recognition on SAR for nano Pt−Ru catalysts and the intrinsic difference of thus-reached conclusions from those of previous approaches.

Figure 5 describes the dependence of A_m on $m_{RuO_xH_y}$. Both MLR and GRNN indicate beneficial effects of hydrous Ru oxides on catalytic activity, which is consistent with experimental observations.[24−26,37] According to the GRNN prediction, the increase speed of A_m would slow at high $m_{RuO_xH_y}$, which is also understandable.

Figure 6 gives the dependence of A_m on ϕ. Because $^1/_\phi$ was used in the modeling, the MLR prediction of A (ϕ; $m_{RuO_xH_y}$, x_{Ru}) takes on a reciprocal curve. From the model predictions, the smaller the particle size, the higher the catalytic activity. No A_m peak can be seen within the model variable range (2−5 nm). According to the GRNN picture, the increase speed of A_m would slow after ϕ decreased below 2.5 nm. The optimal particle size giving a peak A_m should, if it exists, locate outside the model variable range; no attempt was made to predict it with the current model because the behavior of the model prediction beyond the model variable range would become unreliable.

Figure 7 pictures the dependence of A_m on x_{Ru}. MLR predicts that A_m increases with x_{Ru} slightly, whereas GRNN points out a decline trend in A (x_{Ru}; ϕ, $m_{RuO_xH_y}$). Despite the fact that the two results are not quite consistent, one point can still be concluded: the effect of the alloyed degree of nano Pt−Ru catalysts is unremarkable.

It can be found that the experimental data points plotted in Figures 5−7 are rather scattered, especially in Figure 7. This phenomenon is a typical sign of the multivariate effect. Because of the difficulty in singly tuning one structural parameter while other parameters remain unchanged, smooth data distribution can hardly be obtained in practice. It is obvious that true SAR information cannot be attained if single-variate analysis was employed instead of the pattern-recognition method.

3.3. Comparison between the Effects of x_{Ru} and $m_{RuO_xH_y}$. Comparing Figures 5 and 7, one can draw a conclusion strongly supporting the opinion of Rolison et al.,[22−25] that is, in nano Pt−Ru catalysts the preferable form of Ru is RuO_xH_y rather

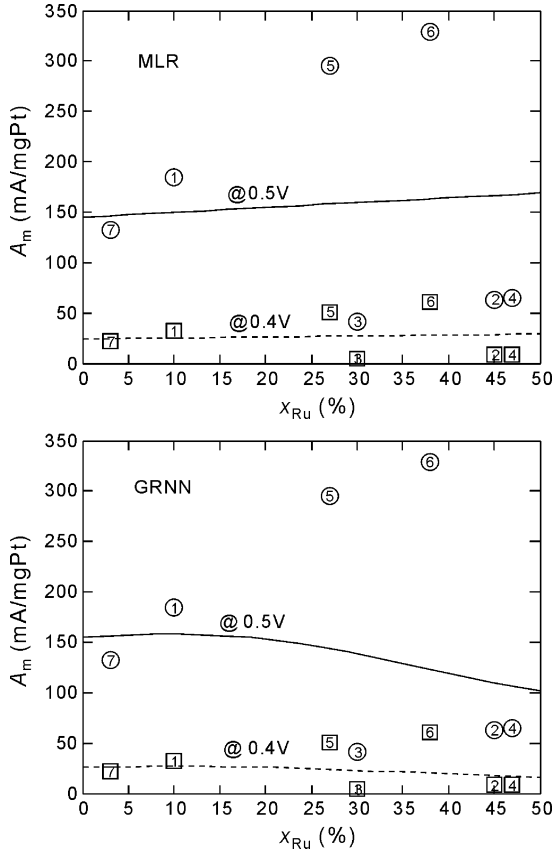

Figure 7. Model prediction A (x_{Ru}; ϕ, $m_{RuO_xH_y}$), describing the explicit dependence of catalytic activity on the alloyed degree with parametrical dependence on ϕ and $m_{RuO_xH_y}$, which took their mean values in this calculation. The discrete points in the figure are the experimental data, and the continuous lines are the model outputs.

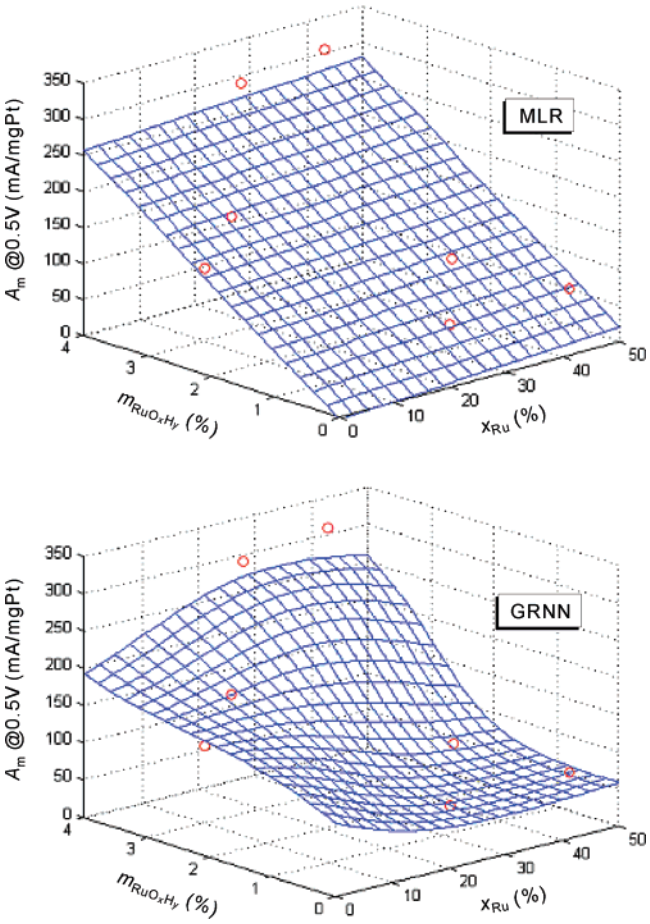

Figure 8. Model prediction A (x_{Ru}, $m_{RuO_xH_y}$; ϕ), showing the relative importance between RuO_xH_y and the alloyed degree. ϕ is held at its mean value in this calculation. The discrete points in the figure are the experimental data, and the continuous meshes are the model outputs.

than Pt−Ru alloy. A (x_{Ru}, $m_{RuO_xH_y}$; ϕ) was simulated and plotted in Figure 8 to further reveal the dependence of A_m on x_{Ru} and $m_{RuO_xH_y}$.

A qualitative conclusion can be obtained from the MLR result: both increasing x_{Ru} and increasing $m_{RuO_xH_y}$ would benefit A_m, but the effect of $m_{RuO_xH_y}$ would be much more significant. GRNN drew a subtler picture: increasing $m_{RuO_xH_y}$ would always be beneficial and significant, whereas the change of x_{Ru} would be less effective and uncertain, and an optimal x_{Ru} might exist in a certain case.

Figure 8 provides some instructive information for catalyst optimization, but the picture is far from precise. If more representative data can be added into the database, then Figure 8 would be very valuable. The database expansion work is now ongoing in our laboratory; subsequent results will be reported elsewhere.

4. Summary

The SAR study of nano Pt−Ru is hindered greatly by the complexity of the microscopic structure of the catalyst. Because the monodependency of A_m on individual structural factors is inaccessible experimentally, a pattern-recognition study seems to be an effective solution to this problem. The purpose of this paper is to advocate the methodology of pattern recognition with illustrative examples to show its intrinsic advantages over previous approaches in the literature. Different from unilateral approaches, the proposed approach sees the multivariate system in perspective. Therefore, the conclusion thus reached is, in essence, different from and more reasonable than previous ones. According to the preliminary results based on a rather limited database, both increasing the content of hydrous ruthenium oxides and decreasing the particle size were found to benefit the catalytic activity, whereas the effect of the alloyed degree turned out to be unremarkable. These conclusions might be modified in the future as the database is expanded by adding more typical samples and possibly more activity-determining factors.

Acknowledgment. This work was supported by the National Key Fundamental R&D Program (TG2000026408), the National Hi-Tech R&D Program (2002AA517030), the Natural Science Foundation of China (20122101, 20433060, 20473058), and the Program for New Century Excellent Talents in University.

Appendixes

1. MATLAB code for MLR modeling

```
% normalization
[Sn Smean Sstd] = prestd(S′);
[An Amean Astd] = prestd(A′);

% multiple linear regression
M = Sn′\An′;

% prediction
Sxn = trastd(Sx′,Smean,Sstd);
Axn = Sxn′*M;
Ax = poststd(Axn′,Amean,Astd)′
```

2. MATLAB code for GRNN modeling

```
% normalization
[Sn Smean Sstd] = prestd(S′);
[An Amean Astd] = prestd(A′);

% generalized regression neural network
M = newgrnn(Sn,An);

% simulation
Sxn = trastd(Sx′,Smean,Sstd);
Axn = sim(M,Sxn);
Ax = poststd(Axn,Amean,Astd)′
```

References and Notes

(1) Carrette, L.; Friedrich, K. A.; Stimming, U. *Fuel Cells* **2001**, *1*, 5.
(2) Aricò, A. S.; Srinivasan, S.; Antonucci, V. *Fuel Cells* **2001**, *1*, 1.
(3) Hogarth, M. P.; Ralph, T. R. *Platinum Met. Rev.* **2002**, *46*, 146.
(4) Wasmus, S.; Küver, A. *J. Electroanal. Chem.* **1999**, *461*, 14.
(5) McNicol, B.; Rand, D.; Williams, K. *J. Power Sources* **1999**, *83*, 15.
(6) Lamy, C.; Leger, J.-M. In *Interfacial Electrochemistry*; Wieckowski, A., Ed.; Marcel Dekker: New York, 1999, *48*, 885.
(7) Reddington, E.; Sapienza, A.; Gurau, B.; Viswanathan, R.; Sarangapani, S.; Smotkin, E. S.; Mallouk, T. E. *Science* **1998**, *28*, 1735.
(8) Gotz, M.; Wendt, H. *Electrochim. Acta* **1998**, *43*, 3637.
(9) Chen, K. Y.; Sun, Z.; Tseung, A. C. C. *Electrochem. Solid State Lett.* **2000**, *3*, 10.
(10) Gurau, B.; Viswanathan, R.; Liu, R. X.; Lafrenz, T. J.; Ley, K. L.; Smotkin, E. S.; Reddington, E. Sapienza, A.; Chan, B. C.; Mallouk, T. E.; Sarangapani, S. *J. Phys. Chem. B* **1998**, *102*, 9997.
(11) Liu, R. X.; Iddir, H.; Fan, Q. B.; Hou, G. Y.; Bo, A. L.; Ley, K. L.; Smotkin, E. S.; Sung, Y. E.; Kim, H.; Thomsa, S.; Wieckowski, A. *J. Phys. Chem. B* **2000**, *104*, 3518.
(12) Jusys, Z.; Schmidt, T. J.; Dubau, L.; Lasch, K.; Jörissen, L.; Garche, J.; Behm, R. J. *J. Power Sources* **2002**, *105*, 297.
(13) Watanabe, M.; Motto, M. *J. Electroanal. Chem.* **1975**, *60*, 275.
(14) McNicol, B. D.; Short, R. T. *J. Electroanal. Chem.* **1977**, *81*, 249.
(15) Yajima, T.; Wakabayashi, N.; Uchida, H.; Watanabe, M. *Chem. Commun.* **2003**, 828.
(16) Hogarth, M. P.; Hards, G. A. *Platinum Met. Rev.* **1996**, *40*, 150.
(17) Franaszczuk, K.; Sobkowski, J. *J. Electroanal. Chem.* **1992**, *327*, 235.
(18) Ley, K. L.; Liu, R. X.; Pu, C.; Fan, Q. B.; Leyarovska, N.; Segre, C.; Smotkin, E. S. *J. Electrochem. Soc.* **1997**, *144*, 1543.
(19) Frelink, T.; Visscher, W.; Cox, A. P.; Veen, J. V. *Electrochim. Acta* **1995**, *40*, 1537.
(20) Andrew, M. R.; Glazebrook, R. W. In *An Introduction to Fuel Cells*; Williams, K. R., Ed.; Elsevier: Amsterdam, 1966, p 127.
(21) Lu, Q.; Yang, B.; Zhuang, L.; Lu, J. *J. Phys. Chem. B* **2005**, *109*, 1715.
(22) Rolison, D. R. *Science* **2003**, *299*, 1698.
(23) Stroud, R. A.; Long, J. W.; Swider-Lyons, K. E.; Rolison, D. R. *Microsc. Microanal.* **2002**, *8*, 50.
(24) Long, J. W.; Stroud, R. M.; Swider-Lyons, K. E.; Rolison, D. R. *J. Phys. Chem. B* **2000**, *104*, 9772.
(25) Rolison, D. R.; Hagans, P. L.; Swider, K. E.; Long, J. W. *Langmuir* **1999**, *15*, 774.
(26) Ren, X. M.; Wilson, M. S.; Gottesfeld, S. *J. Electrochem. Soc.* **1996**, *143*, L12.
(27) Kinoshita, K. *J. Electrochem. Soc.* **1990**, *137*, 845.
(28) Attwood, P. A.; McNicol, B. D.; Short, R. T. *J. Appl. Electrochem.* **1980**, *10*, 213.
(29) McNicol, B. D.; Attwood, P.; Short, R. T. *J. Chem. Soc., Faraday Trans. 1* **1981**, *77*, 2017.
(30) Yahikozawa, K.; Fujii, Y.; Matsuda, Y.; Nishimura, K.; Takasu, Y. *Electrochim. Acta* **1991**, *36*, 973.
(31) Takasu, Y.; Iwazaki, T.; Sugimoto, W.; Murakami, Y. *Electrochem. Commun.* **2000**, *2*, 671.
(32) Kabbabi, A.; Gloaguen, F.; Andolfatto, F.; Durand, R. *J. Electroanal. Chem.* **1994**, *373*, 251.
(33) Frelink, T.; Visscher, W.; van Veen, J. A. R. *J. Electroanal. Chem.* **1995**, *382*, 65.
(34) Gloaguen, F.; Léger, J.-M.; Lamy, C. *J. Appl. Electrochem.* **1997**, *27*, 1052.
(35) Takasu, Y.; Itaya, H.; Iwazaki, T.; Miyoshi, R.; Ohnuma, T.; Sugimoto, W.; Murakami, Y. *Chem. Commun.* **2001**, 341.
(36) Ren, X.; Zelenay, P.; Thomas, S.; Davey, J.; Gottesfeld, S. *J. Power Sources* **2000**, *86*, 111.
(37) Gasteiger, H. A.; Marković, N.; Ross, P. N., Jr.; Cairns, E. J. *J. Phys. Chem.* **1993**, *97*, 12020.
(38) Antolini, E.; Cardellini, F. *J. Alloy Comp.* **2001**, *315*, 118.
(39) Antolini, E.; Cardellini, F.; Giorgi, L.; Passalacqua, E. *J. Mater. Sci. Lett.* **2000**, *19*, 2099.
(40) Lin, S.; Hsiao, T.; Chang, J.; Lin, A. *J. Phys. Chem. B* **1999**, *103*, 97.
(41) Mckeown, A.; Hagans, L.; Carette, L.; Russell, E.; Swider, E.; Rolison, R. *J. Phys. Chem. B* **1999**, *103*, 4825.
(42) Yang, B.; Lu, Q.; Wang, Y.; Zhuang, L.; Lu, J.; Liu, P.; Wang, J.; Wang, R. *Chem. Mater.* **2003**, *15*, 3552.
(43) Zheng, J. P.; Cygan, P. J.; Jow, T. R. *J. Electrochem. Soc.* **1995**, *142*, 2699.
(44) Roth, C.; Goetz, M.; Fuess, H. *J. Appl. Electrochem.* **2001**, *31*, 793.
(45) Dmowski, W.; Egami, T.; Swider-Lyons, K.; Love, C.; Rolison, D. *J. Phys. Chem. B* **2002**, *106*, 12677.
(46) Fu, R.; Ma, Z.; Zheng, J. *J. Phys. Chem. B* **2004**, *106*, 3592.
(47) Radmilović, V.; Gasteiger, H. A.; Ross, P. N., Jr. *J. Catal.* **1995**, *154*, 98.
(48) Gong, S.; Lu, J.; Yan, H. *J. Electroanal. Chem.* **1997**, *436*, 291.